



Local magnitude calibration of seismic events in the West Rand, Far West Rand, and Klerksdorp–Orkney–Stilfontein–Hartebeesfontein gold mining areas

by M.B.C. Brandt

Affiliation:

¹Council for Geoscience
Engineering and Geohazards,
Unit, South Africa.

Correspondence to:

M.B.C. Brandt

Email:

mbrandt@geoscience.org.za

Dates:

Received: 29 Jul. 2021

Revised: 11 Oct. 2021

Accepted: 15 Oct. 2021

Published: November 2021

How to cite:

Brandt, M.B.C. 2021

Local magnitude calibration
of seismic events in the West
Rand, Far West Rand, and
Klerksdorp–Orkney–Stilfontein–
Hartebeesfontein gold mining
areas.

Journal of the Southern African
Institute of Mining and Metallurgy,
vol. 121, no. 11, pp. 573–580

DOI ID:

<http://dx.doi.org/10.17159/2411-9717/1301/2021>

Synopsis

Richter magnitudes for seismic events were calibrated for use as a Local magnitude scale in the West Rand (WR), Far West Rand (FWR), and Klerksdorp–Orkney–Stilfontein–Hartebeesfontein (KOSH) gold mining areas. Richter magnitudes are currently calculated from seismograms recorded by local surface cluster networks using tabulated calibration values for Southern California, published in 1958. The Richter (1958) model is incorrect for distances of less than 30 km and should be applied only to crustal earthquakes in regions with similar attenuation properties to those of Southern California. When compared to the South African National Seismograph Network (SANSN), the cluster networks, on average, overestimate seismic event magnitudes by approximately 0.1 of a magnitude unit. A calibrated Local magnitude scale was derived by means of a multiple regression analysis between the Local magnitudes reported by the SANSN and the largest zero-to-peak trace amplitudes measured on the cluster network horizontal seismograms, after modelling the attenuation of the seismic waves as these progress from the epicentre to the station position. Magnitudes reported by individual stations for the same event show a significant scatter around the average magnitude owing to the near-surface amplifications of the seismic waves at the recordings sites. Average magnitude should be estimated using as many magnitudes of individual stations as possible to ensure an accurate estimate. Larger event magnitudes should be compared with those recorded by the SANSN.

Keywords

Richter magnitude, local magnitude calibration, seismic event, Witwatersrand Basin.

Introduction

Magnitude in seismology is a concept that describes the size of a seismic event based on instrumental measurements of some kind. The first magnitude scale was introduced by Richter (1935) for Southern California, USA. This scale only requires the location of the seismic event to be known and the ground motion amplitudes to be recorded by a standard Wood-Anderson seismograph. The maximum zero-to-peak trace amplitudes of the earthquake signals are measured on both horizontal-component seismograms (NS and EW) and the magnitude is calculated using the greater of the two measurements. Richter (1935) quantified the scale as follows: *'The magnitude of any shock is taken as the logarithm of the maximum trace amplitude, expressed in microns, with which the standard short-period torsion seismometer... would register that shock at an epicentral distance of 100 km.'*

To calculate magnitudes for other distances, Richter (1958) provided tabulated attenuation corrections (calibration values) for distances from 0–600 km, assuming a focal depth of 18 km. Accordingly, Richter magnitude M_L is calculated using the equation:

$$M_L = \log_{10}(A_{\max}) - \log_{10}(A_0) \quad [1]$$

where A_{\max} is the largest measured zero-to-peak trace amplitude in millimetres on a Wood-Anderson recorded horizontal seismogram, A_0 represents the trace amplitudes in millimetres from an earthquake of $M_L=0$, and $-\log_{10}(A_0)$ represents the tabulated calibration values (Richter, 1958). Hutton and Boore (1987) derived the following parametric equation for the calibration values:

$$-\log_{10}(A_0(R)) = 1.11 \cdot \log_{10}(R) + 0.00189 \cdot R - 2.09 \quad [2]$$

where R is the hypocentral distance in kilometres.

Local magnitude calibration of seismic events in the West Rand, Far West Rand

In Equation [2], the largest trace amplitude is measured in nanometres on a synthetic seismogram recorded by a modern horizontal-component seismograph. The seismogram is filtered so that the response of the seismograph and filter system replicates that of a standard Wood-Anderson seismograph, but with a static $1 \times$ magnification. Modern synthetic seismograms more closely resemble the signal recordings than the actual standard Wood-Anderson seismograph because the manufacturer specifications for magnification published in the 1930s were found to be inaccurate (Uhrhammer and Collins, 1990).

Standard Equation [2] should be used when calculating Richter magnitudes for crustal earthquakes in regions with attenuation properties similar to those of Southern California. For regions with different attenuation properties, the standard equation is of the form:

$$M_L = \log_{10}(A_{\max}) + C(R) + D \quad [3]$$

where A_{\max} and R are the same as in Equations [1] and [2] and where $C(R)$ and D need to be calibrated to adjust for the different regional attenuation. The maximum amplitude may be measured on a vertical-component seismogram after adjusting for any systematic differences between the amplitudes recorded by the horizontal seismographs and the vertical seismographs (Bormann, 2012).

The South African national geological survey (the Council for Geoscience) is mandated to operate the South African National Seismograph Network (SANSN). A calibrated Richter magnitude scale, referred to as a Local magnitude scale, was derived using vertical-component seismographs for the SANSN (Saunders *et al.*, 2008; 2012):

$$-\log_{10}A_0(R) = 1.149 \cdot \log_{10}(R) + 0.00063 \cdot R - 2.04 \quad [4]$$

where A_0 and R are the same as before. Vertical-component maximum amplitudes were selected for continuity because, until the 1990s, the SANSN comprised mostly vertical-component seismometers. Dissimilarities in the coefficients for $\log_{10}(R)$ and R in Equations [2] and [4] reflect the different attenuation properties between Southern California and South Africa.

In addition to the SANSN, the Council for Geoscience also operates cluster networks of dense local, surface stations within the Far West Rand (FWR), West Rand (WR), Central Rand, and the Klerksdorp–Orkney–Stilfontein–Hartebeesfontein (KOSH) gold mining areas. The magnitudes reported by the cluster networks have not yet been calibrated. Richter magnitudes are currently calculated using Equation [1] and the tabulated values of Richter (1958) for Southern California. This causes discrepancies between the Local magnitudes reported by the SANSN and Richter magnitudes reported by the cluster networks. On average, the cluster networks overestimate seismic event magnitudes by approximately 0.1 of a magnitude unit. The seismograms recorded by the stations of the cluster networks are automatically processed and manually re-analysed using Antelope 5.4 software (2018). This software calculates Richter magnitudes with the largest zero-to-peak trace amplitudes measured on the horizontal-component seismograms with Equation [1], identical to the original method of Richter (1935). The calibration values in Equation [4] for the vertical-component seismograms of the SANSN that resemble a synthetic Wood-Anderson seismograph with a static magnification $1 \times$ can therefore not be simply transferred to the cluster network.

The purpose of this article is to derive tabulated calibration values for $\log_{10}(A_0)$ in Equation [1] for the cluster network horizontal components such that, on average, the Local magnitudes reported by the cluster networks have the same sizes as those reported by the SANSN. This will be accomplished by means of a multiple regression analysis between the Local magnitudes reported by the SANSN, the largest zero-to-peak trace amplitudes measured on the cluster network horizontal seismograms, where $-\log_{10}(A_0)$ is modelled using Equation [3] and where $C(R) + D$ have the same respective variables as in Equation [2].

Richter magnitudes currently reported by surface mine cluster networks

The Council for Geoscience operates three mine surface cluster networks, and the event origin times, epicentres and magnitudes may be obtained from the web page <<http://196.38.235.147:8070/livemines/>>. The mine and environmental water management programme (MEWMP) network consists of ten stations across the West, Central, and East Rand. The purpose of this network is to monitor seismicity that may be linked to the ingress of water into abandoned mines in and around the City of Johannesburg. The FWR network comprises 11 stations situated in the Carletonville region. The network was installed as part of a research project initiated by the Japanese International Cooperation Agency. The KOSH network consists of 19 stations installed in the Klerksdorp–Orkney–Stilfontein–Hartebeesfontein region, as part of a project sponsored by the Mine Health and Safety Council.

The positions of stations and the seismic events for the period 1 January 2019 to 19 June 2020 used in this study are shown in Figures 1 and 2. The tight clustering of seismic events detected by both the SANSN and the surface cluster network is an artefact of the event density; in other words, most of the events were located at the centre of the cluster. The Richter magnitudes in Figures 1 and 2 were calculated by means of Antelope 5.4 software (2018) using Equation [1] and the calibration values for $\log_{10}(A_0)$, listed in Table I. The calibration values in Table I, as well as those for Equations [2] and [4], are graphically depicted in Figure 3. Richter's equation for the tabulated calibration function $-\log_{10}A_0(\Delta)$ in Table I is derived (Figure 3) by means of a multiple regression analysis for an equation with the same variables as Equation [2]:

$$-\log_{10}A_0(\Delta) = 0.961 \cdot \log_{10}(\Delta) + 0.00272 \cdot \Delta + 0.00272 \cdot \Delta + 0.787 \quad R^2 = 0.983 \quad [5]$$

R^2 is the goodness-of-fit measure where $0 < R^2 < 1$ for the linear regression model, and 1 indicates a perfect fit.

There is a significant offset between the constant value 0.787 and the constants -2.09 and -2.04 in Equation [2] (Hutton and Boore, 1987) and Equation [4] (Saunders *et al.*, 2012), respectively. This is because Richter (1935) measured the largest trace amplitude in millimetres as recorded by a standard Wood-Anderson seismograph, whereas modern simulated Wood-Anderson seismograms have a static amplification of $\times 1$. Unit amplification implicitly means that true ground motion amplitudes in nanometres are measured for the recorded frequency range. Hutton and Boore (1987) updated the coefficients for $\log_{10}(R)$ and R in Equation [2] and determined that Richter's (1958) calibration values for near distance Δ

Local magnitude calibration of seismic events in the West Rand, Far West Rand

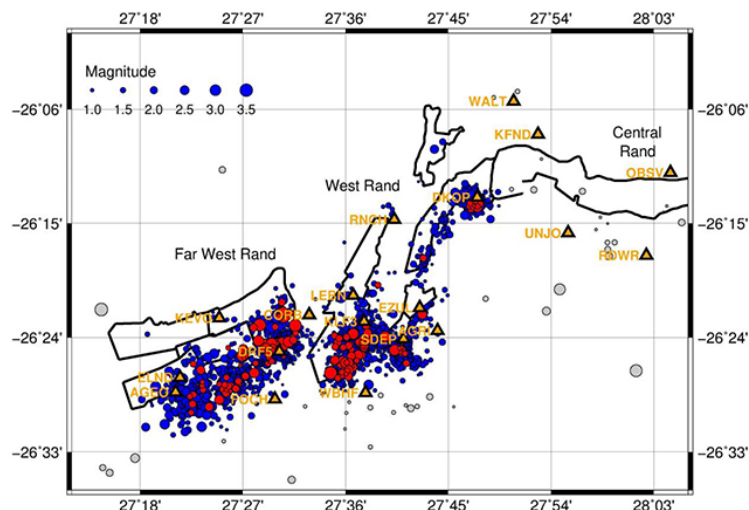


Figure 1—Map of seismograph stations around the WR and FWR and the western part of the Central Rand gold mining areas. Eleven triangles depict the stations of the FWR cluster network and eight triangles depict the WR and western Central Rand's stations of the MEWM cluster network. Station codes are listed in orange. Blue dots represent events from 2019 01 01 to 2020 06 19 located by the two cluster networks in the WR and FWR, and red dots represent events that were also detected by the SANSN. Events outside the mining areas that were rejected from this study are greyed out. Mines are delineated by thick, black lines

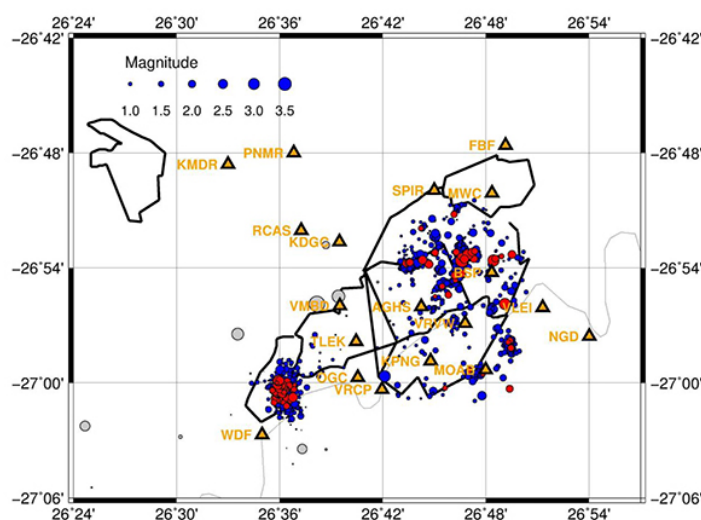


Figure 2—Map of seismograph stations around the KOSH area. The stations are depicted by nineteen triangles. Station codes are listed in orange. Blue dots represent events from 2019 01 01 to 2020 06 19 located by the cluster network in the KOSH area and red dots represent events that were also detected by the SANSN. Events outside the mining area that were rejected from this study are greyed out. Mines are delineated by thick, black lines and the Vaal River is depicted by a thin grey line

<30 km are incorrect (Figure 3). Bakun and Joyner (1984) drew the same conclusion for near-distance weak events recorded in Central California. Richter's 1958 calibration values causes magnitude estimates from nearby stations to be smaller than those from more distant stations (Bormann, 2012). Hutton and Boore (1987) further suggested deriving calibration values based on a shallow focal depth of 0 km for crustal earthquakes, as values measured in this way provide a better fit than those calculated using the 18 km focal depth proposed by Richter (1958).

An orthogonal regression between 256 Local magnitudes reported by the SANSN (Saunders *et al.*, 2012) and the Richter magnitudes reported by the surface cluster networks (Richter, 1958) in Figure 3 produces the equation:

$$M_L(\text{SANSN}) = 0.99 * M_L(\text{cluster}) - 0.12 \quad R^2 = 0.93 \quad [6]$$

where R^2 is defined as before. The cluster networks, on average, overestimate seismic event magnitudes by approximately 0.1 of a magnitude unit. Even though the goodness-of-fit is high and the 95% confidence level indicates a credible match, the scatter of the magnitudes around the best fit orthogonal relation is significant. The scatter is investigated in the histograms and bar graph in Figures 5 and 6. The differences between the Richter magnitudes observed by individual stations of the cluster networks and the average Richter magnitudes calculated for the respective seismic events have a standard deviation of 0.56 (Figure 5). The frequency bar graph in Figure 6 for stations with magnitude differences of more than 0.56 revealed incorrectly calibrated stations AGRI and ELND. The magnitude differences, excluding recordings from stations AGRI and ELND, have a standard deviation of only 0.48. The rejected magnitudes reported by AGRI and ELND cause the distribution of

Local magnitude calibration of seismic events in the West Rand, Far West Rand

Table I

Interpolated tabulated calibration function $-\log_{10}A_0(\Delta)$ to calculate Richter magnitudes using Antelope 5.4 software (2018). The classical values derived by Richter (1958) are shown in bold. A_0 represents the maximum horizontal trace amplitudes in millimetres recorded by a standard Wood-Anderson seismometer from an earthquake of $M_L=0$ at an epicentral distance of Δ km

Δ (km)	$-\log_{10}A_0(\Delta)$						
0	1.4	95	3.0	270	3.9	450	4.6
5	1.4	100	3.0	280	3.9	460	4.6
10	1.5	110	3.1	290	4.0	470	4.7
15	1.6	120	3.1	300	4.0	480	4.7
20	1.7	130	3.2	310	4.1	490	4.7
25	1.9	140	3.2	320	4.1	500	4.7
30	2.1	150	3.3	330	4.2	510	4.8
35	2.3	160	3.3	340	4.2	520	4.8
40	2.4	170	3.4	350	4.3	530	4.8
45	2.5	180	3.4	360	4.3	540	4.8
50	2.6	190	3.5	370	4.3	550	4.8
55	2.7	200	3.5	380	4.4	560	4.9
60	2.8	210	3.6	390	4.4	570	4.9
65	2.8	220	3.65	400	4.5	580	4.9
70	2.8	230	3.7	410	4.5	590	4.9
80	2.9	240	3.7	420	4.5	600	4.9
85	2.9	250	3.8	430	4.6		
90	3.0	260	3.8	440	4.6		

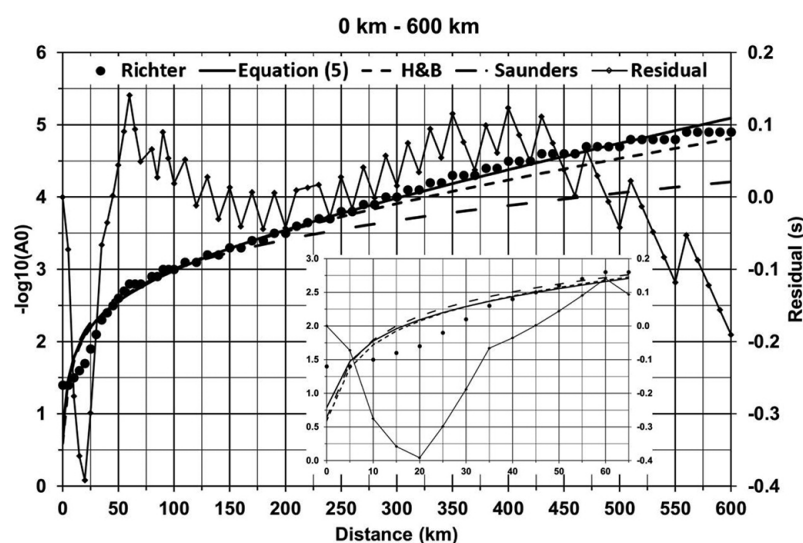


Figure 3—Richter's equation (Equation [5]) (thick solid curve, scale on the left axis) for the tabulated calibration function $-\log_{10}A_0(\Delta)$ in Table I (dots) derived by means of a multiple regression analysis for a model with the same respective variables as in Equation [2]. Residual values between $-\log_{10}A_0(\Delta)$ in Table I and Richter's equation are shown as thin dotted lines with scale on the right axis. This is compared to Equation [2] (Hutton and Boore, 1987), displayed as a short dashed curve and Equation [4] (Saunders et al., 2012), shown as a long dashed curve. Equations [2] and [4] are normalised to $-\log_{10}A_0(\Delta) = 3$ at 100 km distance for direct comparison with Equation [5]. Distances between zero and 65 km are enlarged at the bottom right

the histogram to become more symmetrical in regard to positive magnitude differences, especially for those >0.6 . However, magnitude differences <0.6 also decrease, indicating that stations AGRI and ELND were not malfunctioning throughout the whole study period. Hence, for the remainder of this article, only observations where the Richter magnitude difference is <0.56 will be used.

Next, we investigate whether the finding by Hutton and Boore (1987) and by Bakun and Joyner (1984), that Richter's (1958) calibration values for near distance $\Delta < 30$ km in California are incorrect, can be extrapolated to the WR, FWR, and KOSH mining areas. To accomplish this we plot the Richter magnitude differences (<0.56) as a function of distance in Figure

7. A comparison between the Richter magnitude differences and the residual values between $-\log_{10}A_0(\Delta)$ in Table I and Richter's equation (Figure 3) confirms that Richter's (1958) calibration values are indeed also incorrect for the WR, FWR, and KOSH mining areas for near distances. We conclude that the calibration values for $\log_{10}(A_0)$ should be modelled with Equation [3], where $C(R) + D$ have the same respective variables as in Equation [2]. However, calculating Richter magnitudes with incorrect calibration values for near distances of $\Delta < 30$ km is not the only cause of the large scatter in magnitudes around the best fit orthogonal relation in Figure 4 and the large scatter in the histogram of Richter magnitude differences (Figure 5). The rapid changes of the nine-point running average window

Local magnitude calibration of seismic events in the West Rand, Far West Rand

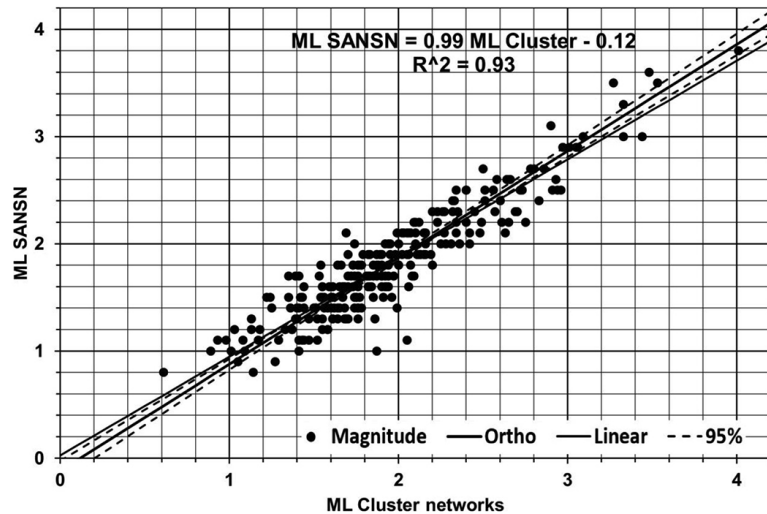


Figure 4—Local magnitudes in the WR, FWR, and KOSH areas reported by the SANSN (Saunders et al. 2012) as a function of Richter (1958) magnitudes reported by the surface cluster networks (dots). The seismic events plotted in this graph correspond to the red dots on the maps in Figures 1 and 2. The equation at the top fits the magnitudes by means of an orthogonal regression (thick line) with goodness-of-fit of 0.93 where the dashed curves represent the 95% confidence interval. This is compared with a linear regression (thin line)

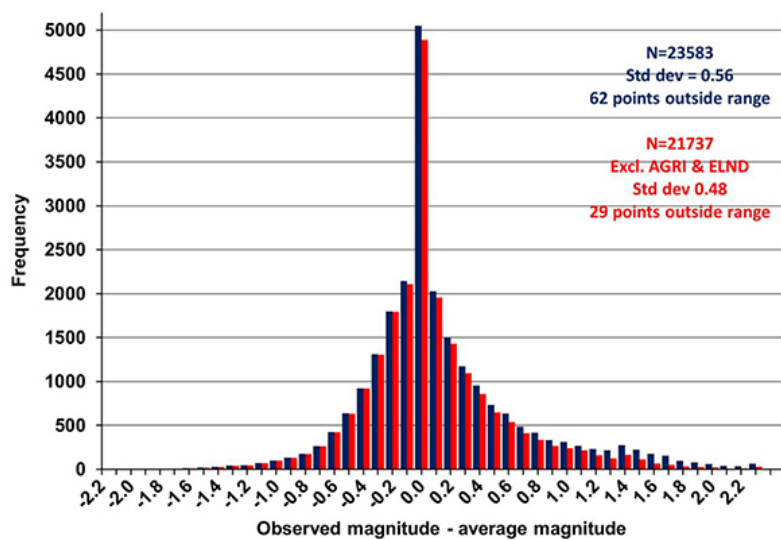


Figure 5—Histogram of the differences between Richter magnitudes observed by individual stations of the cluster networks and the average Richter magnitude calculated for the respective seismic events. The 23 583 magnitude differences used in this study (blue bars) have a standard deviation of 0.56. The 21 737 magnitude differences, excluding recordings from stations AGRI and ELND (red bars – and also see Figure 6) have a standard deviation of 0.48

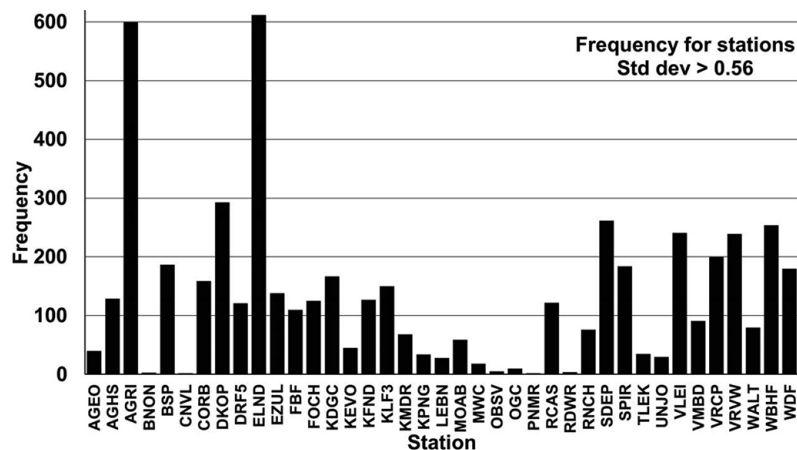


Figure 6 – Frequency of the stations (see maps in Figures 1 and 2, and Figure 5) with magnitude differences >0.56

Local magnitude calibration of seismic events in the West Rand, Far West Rand

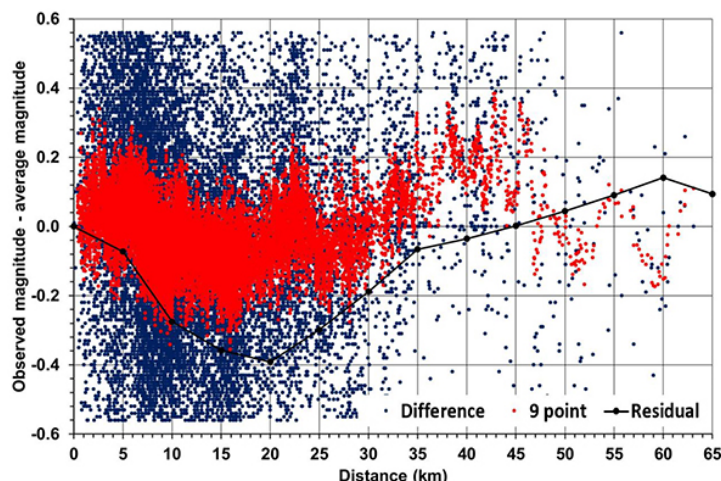


Figure 7—Differences between Richter magnitudes observed by individual stations of the cluster networks and the average Richter magnitude calculated for the respective seismic events as a function of distance (blue dots). Red dots represent a nine-point running average window of the magnitude differences and are compared to the residual values between $-\log_{10}A_0(\Delta)$ in Table I and Richter's equation (Figure 3), which is depicted as thin dotted lines. Richter magnitude differences of more than 0.56 have been excluded from the graph

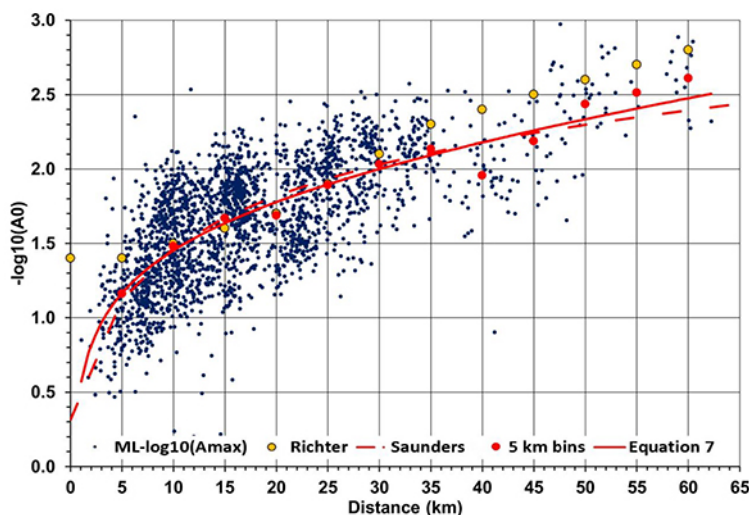


Figure 8—Newly derived calibration function $-\log_{10}A_0(\Delta)$ (red curve), specified in Equation [7] derived by means of a multiple regression for $-\log_{10}A_0(\Delta) = ML - \log_{10}(A_{max})$ (blue dots) for a model with the same variables as in Equation [2]. The average values of $-\log_{10}A_0(\Delta)$ in 5 km bins are shown as large, red dots and Richter's (1958) tabulated values, listed in Table I, as large, orange dots. This is compared with Equation [4] (Saunders et al., 2011), shown as a red, long dashed curve. The constant in Equation [4] was adjusted for an optimum least-squares fit to the values of $-\log_{10}A_0(\Delta)$

between about -0.18 and $+0.1$ at distances of 47 km, 51 km, 55 km and 59 km in Figure 7 indicate that neighbouring stations have observed significantly different magnitudes for the same seismic event. These rapid changes are not visible at shorter distances owing to the many observed magnitudes that plot on top of one another, but which probably also exist. These rapid changes provide evidence of near-surface amplifications where a seismometer has not been installed on competent bedrock. Bormann (2012) reports that the closely spaced stations of a seismic array may measure relative amplifications to one another in ground amplitudes of 10 to 30 times when installed on soft soil such as alluvium. Security is the primary criterion for the selection of a site to install a seismograph station in a mining area as a result of the high risk of theft or vandalism. Many of the seismometers are therefore not installed on competent bedrock, thus providing the option of relocating a station if the security situation worsens or if the host mine or landowner closes or suspends operations. However, magnitude differences

of >0.56 are likely the result of equipment malfunction or processing errors. Antelope 5.4 software (2018) rejects outliers when calculating the average magnitude, and weighs individual magnitude observations according to the signal-to-noise ratio of the maximum measured amplitude.

Local magnitude calibration

Calibration values for $-\log_{10}(A_0)$ in Equation [1] for the cluster networks are derived by means of a multiple regression analysis between the Local magnitudes reported by the SANSN, ML, and the largest zero-to-peak trace amplitudes measured on the cluster network horizontal seismograms, A_{max} , and are shown in Figure 8, with the tabulated values in Table II. The attenuation of the seismic waves as these progress from the epicentre to the station position is modelled with Equation [3] and where $C(R) + D$ have the same variables as in Equation [2]. Values for A_{max} , where the Richter magnitude difference in Figure 5 is >0.56 , were excluded from the analysis.

Local magnitude calibration of seismic events in the West Rand, Far West Rand

Table II

Newly derived tabulated calibration function – $\log_{10}A_0(\Delta)$ obtained from Equation [7] in Figure 8, which was derived by means of a multiple regression analysis. Change reflects the adjustment made to Richter's (1958) tabulated calibration function – $\log_{10}A_0(\Delta)$ listed in Table I

Δ (km)	$-\log_{10}A_0(\Delta)$	Change	Δ (km)	$-\log_{10}A_0(\Delta)$	Change
0	0.55	-0.85	35	2.09	-0.21
5	1.16	-0.24	40	2.18	-0.22
10	1.45	-0.05	45	2.26	-0.24
15	1.64	0.04	50	2.33	-0.27
20	1.78	0.08	55	2.41	-0.29
25	1.90	0.00	60	2.48	-0.32
30	2.00	-0.10			

The derived equation is:

$$0.547 R^2 = 0.473$$

$$-\log_{10}A_0(\Delta) = 0.831 \cdot \log_{10}(\Delta) + 0.00753^* \quad [7]$$

$$\Delta + 0.547 R^2 = 0.473$$

where distance $0 < \Delta < 60$ km and R^2 indicates a poor fit to the large scatter of the values for $-\log_{10}A_0(\Delta) = M_L - \log_{10}(A_{max})$ around the model. The poor fit is unsurprising, given the large scatter of the magnitudes around the best fit orthogonal (Equation [6]) in Figure 4 and the large scatter in Richter magnitude differences (within one standard deviation of 0.56) in Figure 5. However, the average values of $-\log_{10}A_0(\Delta)$ in 5 km bins (Figure 8) compare well with Equation [7] except for the 40 km bin, which may indicate a significant near-site amplification at that distance station compared to most of the seismic events. This shows that good estimates of Local magnitudes by the cluster networks are possible if outliers are rejected and a sufficient number of measurements with appropriate weights for signal-to-noise ratios are averaged, as is currently the practice with Antelope 5.4 software (2018). Most of Richter's (1958) tabulated calibration values are adjusted downward to account for the magnitude overestimate of approximately 0.1 of a unit established in Equation [6] when taking the incorrect model into consideration. This is as expected, since seismic waves show less attenuation with distance in South Africa than is the case in Southern California (Brandt, 2015). The largest adjustment is made at the epicentre, at 0 km distance, in line with the proposal by Hutton and Boore (1987) to derive calibration values for a surface focal depth of 0 km for shallow events as these will provide a better fit for crustal events. This is especially relevant in respect of mine seismic events, where the typical focal depth is 2 km (Brandt, 2014). The newly derived calibration values are similar to those in Equation [4] (Saunders et al., 2012) when adjusted for the constant difference between amplitudes recorded by horizontal seismographs and vertical seismographs.

Discussion and conclusions

Tabulated calibration values $-\log_{10}(A_0)$ were derived for the cluster network horizontal components, such that the Local magnitudes reported by the cluster networks on average have the same sizes as the Local magnitudes reported by the SANSN. This is an improvement on the current situation where the cluster networks, on average, overestimate seismic event magnitudes by approximately 0.1 of a magnitude unit.

The large scatter in magnitudes reported by individual stations for the same event is accounted for by the near-surface amplifications of the seismic waves at the recording sites. Antelope 5.4 software (2018) does not allow for the application of static corrections to the magnitudes of an individual station to compensate for its systematic over- or underestimation in comparison to the average magnitude of an event. The software was selected for its ability to automatically locate large numbers of mining events and to undertake a quick magnitude assessment. This is followed by manual re-analysis with a user-friendly graphical interface and is suitable for processing a large number of events. Even if it were possible to apply a static correction this would not be practical, because stations are re-located if the security at a site deteriorates. Hence, average magnitudes should be calculated from as many as possible individual stations to ensure the best possible magnitude estimates.

Magnitudes for larger events recorded by both the SANSN and cluster networks should be compared to one another. The seismometers of the SANSN are installed on bedrock inside high-quality vaults at sites with low background noise. The SANSN estimates of magnitudes for larger events should therefore be more accurate than those reported by the cluster networks.

Acknowledgements

This research was funded as part of the operation and data analysis of the South African National Seismograph Network and Cluster Mine Networks. The multiple regression analyses for this article were generated by means of the Real Statistics code (Zaiontz, 2020) in Microsoft® Excel® 2016. The maps were drafted using generic mapping tools (Wessel *et al.*, 2013) and graphs were prepared using Microsoft® Excel® 2016. I wish to thank the Council for Geoscience for permission to publish my results. Zahn Nel undertook the language editing. Two anonymous reviewers are thanked for their suggestions to improve the article.

References

- ANTELOPE. 2018. Boulder Real Time Technologies Incorporated. Antelope 5.4. <http://www.BRTT.com>
- BAKUN, W.H. and JOYNER, W. 1984. The ML scale in Central California. *Bulletin of the Seismological Society of America*, vol. 74, no. 5. pp. 1827–1843.
- BORMANN, P. (ed.), 2012. New Manual of Seismological Observatory Practice (NMSOP-2), IASPEI, GFZ German Research Centre for Geosciences, Potsdam. <http://nmsop.gfz-potsdam.de> doi: 10.2312/GFZ.NMSOP-2
- BRANDT, M.B.C. 2014. Focal depths of South African earthquakes and mine events. *Journal of the Southern African Institute of Mining and Metallurgy*. vol. 114. pp. 1–8.
- BRANDT, M.B.C. 2015. Qc and Qs wave attenuation of South African earthquakes. *Journal of Seismology*. doi 10.1007/s10950-015-9536-6
- HUTTON, L.K. and BOORE, D.M. 1987. The ML scale in Southern California. *Bulletin of the Seismological Society of America*, vol. 77. pp. 2074–2094
- RICHTER, C.F. 1955. An instrumental earthquake magnitude scale. *Bulletin of the Seismological Society of America*, vol. 25. pp. 1–32.
- RICHTER, C.F. 1958. *Elementary Seismology*. W. H. Freeman, San Francisco and London. 768 pp.
- SAUNDERS, I., BRANDT, M.B.C., STEYN, J., ROBLIN, D.L., and KIJRO, A. 2008. The South African National Seismograph Network. *Seismological Research Letters*, vol. 79. pp. 203–210. doi: 10.1785/gssrl.79.2.203
- SAUNDERS, I., OTTEMÖLLER, L., BRANDT, M.B.C., and FOURIE, C.J.S. 2012. Calibration of an ML scale for South Africa using tectonic earthquake data recorded by the South African National Seismograph Network: 2006 to 2009. *Journal of Seismology*. doi 10.1007/s10950-012-9329-0
- URRHAMMER, R.A. and COLLINS, E.R. 1990. Synthesis of Wood-Anderson seismograms from broadband digital records. *Bulletin of the Seismological Society of America*, vol. 80. pp. 702–716.
- WESSEL, P., SMITH, W.H.F., SCHARROO, R., LUIS, J.F., and WOBBE, F. 2013. Generic Mapping Tools: Improved version released. *EOS Transactions of the American Geophysical Union*, vol. 94. pp. 409–410.
- ZAIONTZ, C. 2020. Real statistics using Excel. <http://www.real-statistics.com> ◆



Drill and Blast Short Course 2022

23-24 FEBRUARY 2022

ONLINE VIA ZOOM

VENUE: WITS CLUB, JOHANNESBURG

CPD Points

0.1 CPD points for every 1 hour event attended
online or contact

BACKGROUND

There has been a significant change in the explosives and initiating systems used in the mining, quarrying and civil blasting applications both on surface and underground. This short course will provide and align the delegates with some basic principles, tools, examples and understanding of the leverage of these products. Whether you are new to the industry or a seasoned user or find yourself in the position of an explosive manager or supervisor to a regulator, the course will enable some debate, rules and questions you should be asking of your explosive OEM.

The importance of improved safety standards, cost effectiveness and productivity has driven mining management and operators to examine all facets of their operations. Increasingly it has been realised that an efficient drilling and blasting program can impact positively throughout the mining operation from loading to maintenance, hauling to crushing, ground support to scaling and grade control to recovery. We will also test the concepts and increasing challenges of blasting in the vicinity of local communities.

PROGRAMME

'What is an explosive?'

- We will look at the evolution and properties of explosives from Black powder to Ammonium Nitrate, adding fuel oil to make ANFO, packaged explosives and the modern bulk or pumpable technology.

Requirements of an Initiating System

- Where have we come from, safety fuse and how do pyrotechnic detonators (Shock tube) fit to Electronic detonators and their impact on blast design.

Drilling and Blast Design principles

- Reviewing the principles that a well drilled hole is key to a successful blast and what is the relationship to blast geometry.

Blast design principles

- Some simple tools to use, review and calculate your blast design.

Initiation and Timing of Blasts

- Understanding the principles of timing and how this enables us to shape and move the blast muckpile. The addition of control to both manage the uniformity and fragmentation as well as environmental control using electronics.

Specialised Blasting Techniques

- A look into the world of specialised blasting, highwall stability, secondary breaking & demolition.

Environmental and Health

- Managing the community and avoiding the issues of ground vibration, noise & airblast.

PRESENTER



Simon Tose is an expert in Blast Design from AECI and will be sharing his expertise on this subject.

Simon Tose is an established industry recognised consultant, registered professional engineer and leader in technology, mining, explosives and blasting science. Holding a BSC Hons Mining Engineering degree, management and explosive qualifications. Extensive experience in mining methods, education and management of projects and blast investigations. He has written papers, articles and presented at a number of International and Local conferences. Current board member of the IOQSA & ISEE and regular contributions to the SAIMM & AusIMM.

With a strength in project design he leads the Blast Consult team with a strong passion for the development of environmental and blast monitoring, measurement and investigation, consulting, management and financial analysis for AECI

FOR FURTHER INFORMATION, CONTACT:

Camielah Jardine, Head of Conferencing

E-mail: camielah@saimm.co.za | Tel: +27 11 834-1273/7 | Web: www.saimm.co.za



SAIMM
THE SOUTHERN AFRICAN INSTITUTE
OF MINING AND METALLURGY